J Porous Mater (2014) 21:827–837
DOI 10.1007/s10934-014-9832-5

Optimizing the synthesis and properties of Al-modified anatase catalyst supports by statistical experimental design

Rebecca E. Olsen · Calvin H. Bartholomew · David B. Enfield · John S. Lawson · Nathaniel Rohbock · B. Sterling Scott · Brian F. Woodfield

Published online: 20 August 2014

Abstract The important variables in the synthesis of stable, high surface area, aluminum-modified anatase TiO_2 catalyst supports were identified and optimized using statistically designed experiments (DOEs). The first DOE examined ten variables at two levels and a second DOE studied eight variables at three levels. Equations were developed to predict the conditions to obtain the highest surface area and pore volume at the desired pore diameter and predict the pore diameter range that may be obtained. Confirmation trials closely matched predicted surface areas, pore volumes, and pore diameters in all but one trial. Rinsing order (before or after calcination) was the most significant factor. Other important factors were calcination temperature, mol% aluminum, and water addition speed. The results of this study demonstrate (a) the power of DOEs in identifying and controlling synthesis variables in relatively few experiments and (b) how analysis of factor effects can provide insight into the formation mechanism.

Keywords Anatase · Definitive screening · Statistical design · Catalyst support · High surface area

1 Introduction

TiO_2 is an excellent support material for metal and metal oxide catalysts in a number of oxidative synthesis and pollution-control reactions e.g. oxidation of CO at low temperatures [1], preferential oxidation of CO in H_2/CO mixtures [2], low-temperature, direct synthesis of hydrogen peroxide [3], complete oxidation of volatile organic compounds [4], and also as a support and promoter for vanadium oxide in selective catalytic reduction of NO_x [5]. These and other reactions involving catalysts supported on TiO_2 have been reviewed elsewhere [6]. Each application requires specific anatase or anatase/rutile properties such as surface area, pore volume, and pore diameter. Given the complexity involved in preparing catalyst supports, many synthesis variables are expected to affect these properties. Optimizing anatase supports has been the subject of much research; however, most studies have used a traditional approach of varying one factor at a time while holding all other factors constant. Results from the one factor at a time approach are often misleading and inconclusive because (a) only a small amount of the factor space is covered, (b) interactions between factors are unaccounted for, (c) statistical relevance of data is unknown, and (d) full analysis of all synthesis parameters using this approach is nearly impossible due to the large number of experiments required.

Statistically designed experiments (design of experiments or DOEs) are excellent tools to identify factor effects and interactions and determine conditions needed to obtain the desired properties in a minimum number of

Electronic supplementary material The online version of this article (doi:10.1007/s10934-014-9832-5) contains supplementary material, which is available to authorized users.

R. E. Olsen · D. B. Enfield · B. F. Woodfield (✉)
Department of Chemistry and Biochemistry, Brigham Young University, Provo, UT 84602, USA
e-mail: Brian_Woodfield@byu.edu

C. H. Bartholomew
Department of Chemical Engineering, Brigham Young University, Provo, UT 84602, USA

J. S. Lawson · N. Rohbock · B. S. Scott
Department of Statistics, Brigham Young University, Provo, UT 84602, USA

experiments. A few DOEs have been used to study catalysts and catalysts supports, primarily to optimize catalytic processes or the synthesis and dispersion of the catalyst onto a support, as opposed to studying the properties of the support itself [7–13]. While making an important contribution, these studies have nonetheless had a limited impact in the methodology used in the catalysis community. Thus, the majority of work on catalyst preparation continues to use a one factor at a time approach. The limited impact may be due to (a) narrow audiences of journals in which they were published, (b) the limited scope of variables studied (generally studying four variables or less) and therefore failed to demonstrate the advantages of DOEs relative to a conventional design, and (c) a general lack of knowledge of new statistical methods. Nevertheless, the benefits of using DOEs in the study of process variables are dramatic and clear, but this has yet to be demonstrated effectively in the literature. To our knowledge, there are no previously published studies using statistically designed experiments to optimize the synthesis of anatase catalyst supports.

We recently described a simple method which enables preparation of anatase catalyst supports of high surface area and unusually high thermally stable. Moreover, this method enables preparation of anatase having a wide range of pore properties [14]. While this method is relatively simple, more than ten variables must be optimized to maximize surface area and pore volume, and to control pore diameter. Since analyzing variables individually is inefficient and ineffective, two DOEs, (1) a traditional fractional factorial design and (2) a definitive screening design (DSD), were used to optimize surface area and pore volume, and to control pore diameter in a reasonable number of experiments. Traditional fractional factorial designs are among the most widely used DOEs, however, main effect factors are often confounded with one or more two-factor interactions, requiring further experimentation (as observed in this work). Screening designs are useful in assessing the relative impact of a large number of factors in relatively few trials; however, most screening models only allow for a two-level system (three-level is necessary to assess the curvature in the factor-response relationship) and also face problems with confounded interactions. The DSD used in this study is based on a new model proposed by Jones and Nachtsheim [15] which allows for the study of many factors at three levels in only $2k + 1$ (k = number of factors) experiments. DSD is a one-step alternative to other two step DOEs because it can be used to estimate (1) main effects while avoiding any confounded second-order effects, (2) two factor interactions, and (3) the full quadratic model in any three factors, thereby rendering further experimentation unnecessary in most cases. DSD was awarded the American Statistical Association's 2012 Statistics in Chemistry Award for a collaboration using this design to optimize catalytic sequestration of CO_2 and one example of applying DSD to a physical system, characterizing a protein-crosslinking reaction [16], has been published in the public literature, however, DSD is still generally unknown.

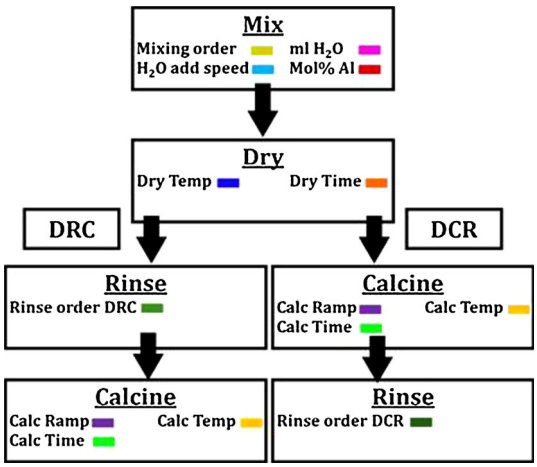

Scheme 1 Synthesis schematic. DRC rinsing order = dry, rinse, calcine. DCR rinsing order = dry, calcine, rinse

In this study we show that through the use of DOEs (a) the surface area and pore structure of anatase supports can be predicted and (b) unusually high surface areas and thermal stabilities can be realized. This work also demonstrates the successful use of DSD to separate and identify the effects of ten variables with no confounded interactions, an approach that is generally applicable to materials and process optimization.

2 Experimental

2.1 Sample preparation

Samples were prepared following a general solvent deficient method that can be used to synthesize many metal and mixed metal oxides [14, 17]. A schematic of the synthesis is found in Scheme 1. Approximately 3.0 ml $TiCl_4$, 0.54 g $Al(NO_3)_3{\cdot}9H_2O$ and 9.1 g NH_4HCO_3 (ABC) were mixed together (amounts listed are for a 5 mol% Al-modified anatase, 5–25 mol% Al ratios were examined). The order in which starting materials were mixed was varied in design of experiment (DOE) 1 but held constant in DOE 2 ($TiCl_4$ and $Al(NO_3)_3{\cdot}9H_2O$ mixed together in a mortar and pestle for 1 min, after which ABC was added and mixed for an additional minute). Distilled H_2O was added in the amount and at the speed outlined in the DOEs 1 and 2. The slurry was then mixed for 5 min to form a

Table 1 Factors and levels for DOE 1 and DOE 2

Factor	Variables	Levels DOE 1	Levels DOE 2
[a]A	Mixing Order	Ti/Al, Al/ABC	Ti/Al
[b]B	Speed of H2O Addition	S, F	S, M, F
C	ml H2O	7, 25	5, 20, 35
[c]D	Order of Rinsing	DRC, DCR	DRC, DCR
E	Drying Time (hrs)	3, 24	3, 14, 24
F	Drying Temp (°C)	25, 100	25, 63, 100
G	Calcination Ramp rate (°C /min)	2, 20	2, 12, 22
H	Calcination Temp (°C)	400, 700	400, 550, 700
I	Calcination Time (hrs)	2, 20	2, 11, 20
J	Mol% Al	5, 22	5, 15, 25

S slow, *M* medium, *F* fast

[a] Ti/Al = $TiCl_4$ + $Al(NO)_3{\cdot}9H_2O$, then ABC. Al/ABC = $Al(NO)_3{\cdot}9H_2O$ + ABC, then TiCl4. ABC = NH_4HCO_3. Held constant in DOE 2 at $TiCl_4/Al(NO)_3$

[b] *DRC* dry, rinse, calcine, *DCR* dry, calcine, rinse. DOE 2 separated into DRC experiments and DCR experiments

Table 2 DOE 1 design and results

	A	B	C	D	E	F	G	H	I	J	Crystallite diameter (nm)	Surface area (m^2/g)	Pore volume (cm^3/g)	Pore diameter (nm)[a]
1	1	Slow	7	DRC	24	25	2	700	2	5	18	50	0.11	6.4
2	2	Slow	7	DRC	3	25	20	700	20	22	9	67	0.12	5.7
3	1	Fast	7	DRC	3	100	2	700	20	22	14	104	0.21	6.1
4	2	Fast	7	DRC	24	100	20	700	2	5	12	61	0.16	7.6
5	1	Slow	25	DRC	3	100	20	400	2	22	2	375	0.33	3.5
6	2	Slow	25	DRC	24	100	2	400	20	5	6	332	0.35	3.5
7	1	Fast	25	DRC	24	25	20	400	20	5	8	203	0.20	3.7
8	2	Fast	25	DRC	3	25	2	400	2	22	6	177	0.31	6.5
9	1	Slow	7	DCR	3	100	20	400	20	5	8	123	0.36	10.1
10	2	Slow	7	DCR	24	100	2	400	2	22	2	369	0.31	3.6
11	1	Fast	7	DCR	24	25	20	400	2	22	6	169	0.52	15.6
12	2	Fast	7	DCR	3	25	2	400	20	5	8	150	0.49	12.3
13	1	Slow	25	DCR	24	25	2	700	20	22	8	124	0.41	12.1
14	2	Slow	25	DCR	3	25	20	700	2	5	10	95	0.46	17.3
15	1	Fast	25	DCR	3	100	2	700	2	5	10	308	0.84	14.9
16	2	Fast	25	DCR	24	100	20	700	20	22	10	94	0.41	15.3

Mixing order 1: ABC & $AlNO_3$, mixing order 2:$TiCl_4$ & $AlNO_3$

[a] Pore diameters calculated from the adsorption branch using a cylindrical method

stabilized anatase precursor. For DRC samples, the slurry was dried in air, rinsed with 2 l of distilled water using a vacuum filtration system at room temperatures, and then immediately calcined. For DCR samples, the slurry was dried in air, calcined, rinsed with 2 l of distilled water using a vacuum filtration system at room temperatures, and subsequently dried 100 °C for 24 h. Drying temperatures and times as well as calcination temperatures, times, and ramp rates were specified by DOEs 1 and 2 and are listed in Tables 2, 3 and 4.

Table 3 DOE 2 (rinsing order DRC) design and results

	B H_2O add speed	C H_2O (ml)	E Dry time (hrs)	F Dry temp (°C)	G Calc ramp (°C/min)	H Calc temp (°C)	I Calc Time (hrs)	J Mol% Al	Crystallite diameter (nm)[a]	Surface area (m^2/g)	Pore volume (cm^3/g)	Pore diameter (nm)[b]
1	Medium	20	14	63	12	550	11	0.15	8	246	0.31	5.4
2	Fast	5	24	63	22	700	2	0.05	11	63	0.15	11.4
3	Medium	35	3	25	22	400	2	0.05	2–3, A	219	0.23	4.4
4	Medium	5	24	100	2	700	20	0.25	9	194	0.25	5.4
5	Fast	20	24	25	2	400	2	0.25	2, A	363	0.28	3.8
6	Fast	35	3	100	12	700	2	0.25	8	130	0.26	11.4
7	Slow	35	24	25	22	700	11	0.25	8	128	0.25	9.5
8	Slow	35	24	100	2	550	2	0.05	7	142	0.23	5.9
9	Fast	35	24	100	22	400	20	0.15	6	334	0.39	3.9
10	Fast	5	3	25	22	550	20	0.25	9	112	0.23	10.1
11	Slow	5	24	25	12	400	20	0.05	9	240	0.22	3.6
12	Slow	5	3	25	2	700	2	0.15	9	83	0.13	8.1
13	Slow	35	3	63	2	400	20	0.25	2, A	394	0.37	4.3
14	Fast	5	3	100	2	400	11	0.05	9	209	0.21	4.5
15	Fast	35	14	25	2	700	20	0.05	12	58	0.16	14.1
16	Slow	5	14	100	22	400	2	0.25	2, A	450	0.36	4.2
17	Slow	20	3	100	22	700	20	0.05	12	60	0.16	12.9

Dry, rinse, calcine synthesis route

[a] A = fairly amorphous according to XRD due to small crystallite sizes. TEM ring patterns confirm some level of crystallinity

[b] Pore diameters of samples 3, 5, 9, 11, 13, 14, and 16 were calculated from the adsorption branch using a cylindrical model. All other pore diameters were calculated from the desorption branch using the SPG (slit) model

2.2 Statistical design

2.2.1 *DOE 1: preliminary screening experiments*

Ten synthesis variables that may affect the surface area, pore diameter, and pore volume of Al-modified anatase were identified based on previous experiments and are listed in Table 1. To study all 10 factors at two levels each in a full factorial design would require $2^{10} = 1{,}024$ experiments. Instead, a 1/64th fractional factorial resolution III minimum aberration experiment (2^{10-6}_{III}) was used for screening [18]. The design and resulting data are shown in Table 2. The design is listed in the standard order but experiments were performed in a random order to prevent biases and to justify the validity of results.

2.2.2 *DOE 2: definitive screening experiments*

Following the preliminary resolution III fractional factorial DOE 1, a DSD was used [15]. This design requires only $2k + 1$ experiments to study k factors at three levels. Based on results from DOE 1, Factor A, mixing order, was held constant ($TiCl_4$ was first mixed with $Al(NO_3)_3{\cdot}9H_2O$) and Factor D was separated into two trials, dry-rinse-calcine (DRC) and dry-calcine-rinse (DCR). The remaining eight factors (B, C, E, F, G, H, I, and J) were studied in 17 experiments for both levels of Factor D-order of rinsing. The design and results are shown Tables 3 and 4. Surface area, pore diameter, and pore volume were analyzed using Jmp Pro version 10 [15, 19–21].

2.3 Sample characterization

X-ray diffraction patterns were collected using a PANalytical X'Pert Pro diffractometer ($Cu–K_{\alpha 1}$ radiation, $\lambda = 1.540598$ Å) at 45 kV and 40 mA over the 2θ range of 10–90° at scanning rates of 0.30–0.44°/min. Average crystallite diameters were estimated using the Scherrer equation and confirmed using transmission electron microscopy (TEM) [22]. TEM measurements were performed on a Tecnai F20 Analytical STEM operating at 200 keV. The samples were dispersed in ethanol and deposited on copper grids (lacey carbon fiber, 400 mesh copper grids, Ted Pella, Inc.).

Full-range N_2 sorption isotherms were collected at 77 K using a Micromeritics TriStar 3020 surface analyzer. Samples of 0.25–0.50 g were degassed at 200 °C for 12–24 h prior to collecting data. Pore volumes were calculated from the adsorption isotherm at a relative pressure of 0.98 and specific surface areas were calculated using the Brunauer–Emmett–Teller (BET) method from a P/P^0 range

Table 4 DOE 2 (rinsing order DCR) design and results

	B H_2O add speed	C H_2O (ml)	E Dry time (h)	F Dry Temp (°C)	G Calc Ramp (°C/min)	H Calc Temp (°C)	I Calc Time (h)	J Mol% Al	Crystallite diameter (nm)	Surface area (m^2/g)	Pore volume (cm^3/g)	Pore diameter (nm)[a]
1	Fast	5	3	100	2	400	11	0.05	8	127	0.38	10
2	Slow	5	14	100	22	400	2	0.25	6	190	0.33	6.6
3	Fast	5	3	25	22	550	20	0.25	11	102	0.34	11.2
4	Slow	20	3	100	22	700	20	0.05	10	82	0.36	14.6
5	Slow	35	24	25	22	700	11	0.25	10	133	0.34	8.5
6	Slow	35	24	100	2	550	2	0.05	8	137	0.39	9.3
7	Medium	35	3	25	22	400	2	0.05	7	139	0.41	10.3
8	Fast	35	24	100	22	400	20	0.15	7	138	0.44	18.6
9	Slow	5	24	25	12	400	20	0.05	7	140	0.45	11.0
10	Fast	5	24	63	22	700	2	0.05	11	81	0.34	15.3
11	Slow	5	3	25	2	700	2	0.15	8	126	0.40	11.8
12	Fast	35	14	25	2	700	20	0.05	13	97	0.41	13.3
13	Medium	5	24	100	2	700	20	0.25	6	148	0.38	9.0
14	Medium	20	14	63	12	550	11	0.15	7	119	0.34	12.5
15	Slow	35	3	63	2	400	20	0.25	6	192	0.44	7.8
16	Fast	20	24	25	2	400	2	0.25	6	182	0.56	16.9
17	Fast	35	3	100	12	700	2	0.25	7	137	0.52	14.0

Dry, calcine, rinse synthesis route

[a] Pore diameters were calculated from the desorption branch using the SPG (slit) model

of 0.05–0.2. H2 type pore diameters were calculated using a modified Pierce method with structural corrections for pore area and volume [23, 24]. H3 and H2/H3 hybridized pore widths were calculated using the newly developed SPG model involving slit geometry for the Kelvin equation, which also incorporates structural corrections for area and volume [25]. For a more detailed discussion see Ref. [25]. For ease of discussion, pore widths and pore diameters will both be referred to as pore diameters. Pore diameters were calculated from either adsorption or desorption branches, depending on the shape of the hysteresis loop. For example, adsorption branch calculations are considered more accurate for H2 type pores, since evaporation of the condensate during desorption is significantly constrained and delayed by the pore necks with "ink-bottle" pore geometry and the connectivity of the network [26–29]. For H3 type hysteresis with slit-like pores, the desorption branch is preferred due to delayed condensation observed in the adsorption process [30–33].

3 Results

3.1 XRD and TEM

XRD data confirms all materials are anatase TiO_2. Crystallite diameters calculated using the Scherrer formula range from 2 to 20 nm for different samples, each have a tight crystallite size distribution and are in good agreement with TEM micrographs (see Tables 2, 3, 4). XRD and TEM reveal changes in crystallite size and pore structure after samples are rinsed prior to rather than after calcination (Tables 2, 3, 4). These changes as well as the statistical analysis of DOE 1 led us to separate the DRC and DCR routes into separate experiments.

3.2 Pore diameter calculations

Pore diameters for DOE 1, DOE 2, and the confirmatory experiments are listed in Tables 2, 3, 4 and 5. All materials were Type IV mesoporous materials with no evident microporosity. Pore diameters in DOE 1 were calculated using the adsorption branch from the modified Pierce model (cylindrical pore model) [23, 24]. Pore diameters in DOE 2 were calculated using either the cylindrical model or, the newly developed SPG (slit) model based on the hysteresis of the isotherms as well as mesopore geometry evident in TEM micrographs [25]. In most cases, calculations from both models agreed well; however, data from several samples were clearly best fitted with either a cylindrical or slit model. Isotherms of DCR materials were mainly H3 associated with slit-like pores (Fig. 1); thus, pore diameters were calculated from the desorption branch using the SPG model [25, 30–33]. Two types of isotherms

Table 5 Experimental conditions for confirmatory trials

Route	Trial	B	C	E	F	G	H	I	J
DRC	1	1	35	24	100	22	400	2	17
	2	1	35	24	100	22	400	2	25
	3	3	35	3	25	22	700	2	17
	4	2	35	24	25	22	400	2	17
	5	1	35	13	65	22	552	2	17
DCR	6	1	35	24	100	22	400	2	17
	7	1	35	24	100	22	400	2	25
	8	3	35	3	25	22	700	2	17
	9	2	35	24	25	22	400	2	17
	10	1	35	13	65	22	552	2	17

DRC dry, rinse, calcine, *DCR* dry, calcine, rinse

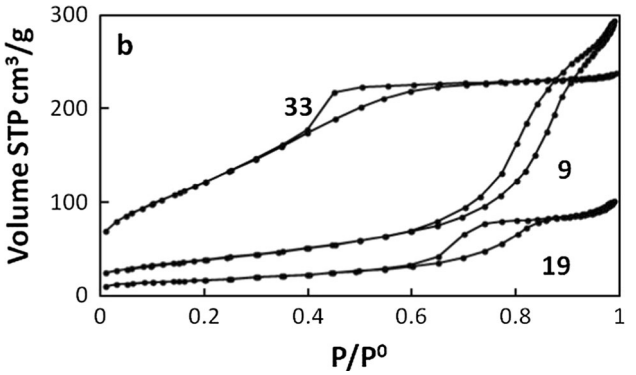

Fig. 1 Isotherm examples. Sample 9 (H3 type, slit-like pores) is representative of DCR materials. Sample 19 (H2/H3 hybridized, irregular channel-like pores) and sample 33 (H2 type, ink-bottle pores) are representative of the two types of pore structures observed in DRC samples. The range of pore structures demonstrates the importance of model selection in pore diameter analysis

were observed for DRC, H2 (samples calcined at 400 °C) and H2/H3 hybridized (samples calcined at 550 and 700 °C; Fig. 1). H2 hysteresis is associated with networked, ink-bottle pores; accordingly, these pore diameters were calculated from the adsorption branch using a cylindrical model to avoid problems associated with percolation encountered in the desorption branch [26–29]. H2/H3 hybridized hysteresis is likely due to a connected, channel-like, irregular pore structure [14]. There is no evidence in the isotherms of delayed condensation or percolation; therefore, pore diameters were calculated from both the adsorption branch and desorption branch using the SPG model. The adsorption branch gives information on the wider pore regions and the desorption branch gives information on constricted regions [14]. To simplify the statistical analysis only the adsorption branch calculations were used. Three samples, DRC samples 5, 9, and 13, exhibited bimodal pore size distributions. Again, to simplify the statistical analysis, only the smaller diameter, which had the largest volume in each case, was used.

3.3 Statistical analysis

3.3.1 DOE 1

A set of traditional screening experiments (Table 2) was designed, conducted, and analyzed to identify which of the ten synthesis factors (Table 1) might have the largest effects on the surface area, pore diameter, and pore volume of Al-modified anatase supports. Factor effects and directions determined in DOE 1 can be found in the Supplementary Information, Table S1. A positive direction indicates increasing the factor level causes an increase in the response while a negative direction indicates increasing the factor level causes a decrease in the response. The factors with the largest effects were identified to be rinsing order (D), calcination temperature (H), amount of H_2O (C), speed of H_2O addition (B), and drying temperature (F), while mixing order (A) exhibited a negligible effect. Because of the highly fractional nature of the design, many factors and two-factor interactions were confounded (i.e. inseparable) and follow-up experiments were necessary to fully confirm the presence, size, and direction of significant effects and to develop models to predict synthesis conditions necessary to produce anatase with various properties. Mixing order (A) was eliminated from further study and was held constant in DOE 2. Rinsing order (D) exhibited a large effect and therefore, two separate studies, in which rinsing order was held constant, were conducted in DOE 2.

3.3.2 DOE 2

DOE 2 was designed and conducted to clarify ambiguity observed in DOE 1. A DSD was used because they are particularly efficient at separating large effect factors from many small effect factors without any confounded interactions in a small number of experiments. Eight factors (B, C, E, F, G, H, I, and J) were studied at three levels, with 17 trials for both mixing orders DRC and DCR, totaling 34 trials. Experimental design and results are listed in Tables 3 (DRC) and 4 (DCR).

Regression models were used fit Eqs. (1)–(6) to the data from the DSDs using JMP Pro Version 10®. Initially forward stepwise regression was used with the combine option and the minimum BIC criterion. The model candidates were the linear, quadratic and linear by linear interactions of factors B–J shown in Tables 3 and 4. It is known that over-fitting is a possibility with forward selection procedures, therefore insignificant terms were eliminated from the models using the backward step procedure. The terms

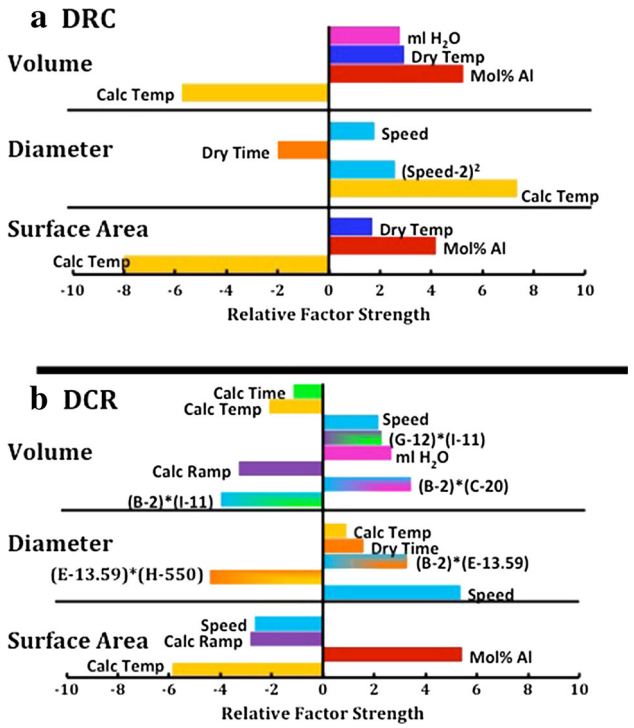

Fig. 2 Factors and interactions that significantly affect the surface area, pore diameter, and pore volume of **a** DRC and **b** DCR materials based on DOE 2 results. A positive direction indicates increasing the factor level causes an increase in the response while a negative direction indicates increasing the factor level causes a decrease in the response. Factor labels: *B, speed* H_2O addition speed, *C* ml H_2O, *E* dry time, *G* calcination ramp rate, *H* calcination temperature, *I* calcination time

included in the models were also compared to the terms found using a Bayesian variable selection (BVS) procedure [34] using weak heredity priors as implemented in the Excel® Add-in BUGSXLA [35] that calls WinBUGS [36]. Since the terms found by both of these methods were in reasonable agreement, the profiler in JMP was used to select conditions for confirmatory experiments that would result in a range of pore volume, pore diameter, and surface area conditions. The profiler was also used to get predicted values and 95 % confidence intervals on the predicted values at these conditions.

Equations (1)–(6) are valid within the range of the factors tested, and predictions outside these ranges may be inaccurate. R^2 measures the variation in observed responses. Standard deviations of the experimental error were estimated from the mean squared errors. Figure 2 shows the relative importance of the factors in the prediction equations. Results from DOE 1 agree somewhat with the results from DOE 2. However, the confounding between main effects and interactions in DOE 1 were eliminated in DOE 2, due to the nature of the DSD, and this resulted in much clearer estimates of the factor effects and allowed development of prediction equations. Specific factor effects are described below.

3.3.3 Surface area

Relative factor strengths and directions are summarized in Fig. 2 and maximum surface areas are predicted to be 389 m^2/g (DRC route) and 195 m^2/g (DCR route) (Eqs. 1, 2). Surface area increased with increasing mol% Al or decreasing calcination temperature for both DRC and DCR samples. In addition to these factors, surface area of DRC samples increased with increasing drying temperature, and surface area of DCR samples increased with decreasing H_2O addition speed or decreasing calcination ramp rate. No other factors or interactions significantly affected surface area. Prediction Eqs. (1) and (2) can be used to predict the surface area expected under various synthesis conditions.

$$\begin{aligned} &DRC\ Surface\ Area\ (m^2/g) \\ &\quad = 471.33 + 0.06024\,(drying\ temp) - 0.71074\,(calc\ temp) \\ &\quad + 555.99\,(mol\%Al) \\ &R^2 = 0.866 \quad standard\ deviation = \pm 118 \end{aligned} \tag{1}$$

$$\begin{aligned} &DCR\ Surface\ Area\ (m^2/g) = 215.0751 \\ &\quad - 9.7753\,(H_2O\ add\ speed) - 1.0464\,(calc\ ramp) \\ &\quad - 0.14456\,(calc\ temp) + 199.946\,(mol\%Al) \\ &R^2 = 0.868 \quad standard\ deviation = \pm 46 \end{aligned} \tag{2}$$

3.3.4 Pore diameter

Figure 2 shows the relative factor strengths and directions. Predicted pore diameters that may be obtained using this technique range from 1 to 12 nm (DRC) and 8–18 nm (DCR) (Eqs. 3, 4). Pore diameters for DCR materials are expected to be larger on average compared with DRC materials. In addition to rinsing order, calcination temperature, H_2O addition speed, and drying time significantly affected pore diameter. A quadratic effect for H_2O addition speed was significant for DRC samples, while interactions between drying temperature and H_2O addition speed, and drying temperature and calcination temperature were observed for DCR samples. Pore diameters of DRC samples are predicted to be minimized using a medium H_2O addition speed, long drying time, and low calcination temperature. Pore diameters of DCR samples are predicted to be minimized using a slow H_2O addition speed, short dry time, and low calcination temperature. Prediction Eqs. (3) and (4) and may be used to understand interactions between factors and predict the pore diameter expected for various synthesis conditions.

$$\begin{aligned} DRC\ Pore\ Diameter\,(nm) &= -6.962 \\ &+ 0.7664\,(H_2O\ add\ speed) - 0.0871\,(dry\ time) \\ &+ 0.02104\,(calc\ temp) + 2.6467\,(H_2O\ add\ speed - 2)^2 \\ R^2 &= 0.85 \quad standard\ deviation = \pm 3.96 \end{aligned} \tag{3}$$

$$\begin{aligned} DCR\ Pore\ Diameter\,(nm) &= 5.3702 \\ &+ 2.1347\,(H_2O\ add\ speed) + 0.06015\,(dry\ time) \\ &+ 0.000244\,(calc\ temp) + 0.1364473 \\ &\quad (H_2O\ add\ speed - 2) \times (dry\ time - 13.5882) \\ &- 0.001222\,(dry\ time - 13.5882) \times (calc\ temp - 550.0) \\ R^2 &= 0.861 \quad standard\ deviation = \pm 3.8 \end{aligned} \tag{4}$$

3.3.5 Pore volume

The relative factor strengths and directions can be seen in Fig. 2 maximum pore volumes are predicted to be 0.39 cm^3/g (DRC route) and 0.59 cm^3/g (DCR route; Eqs. 5, 6). The order of rinsing exhibited a large effect on pore volume and pore volumes of DCR materials are expected to be larger on average compared with DRC materials. In addition to the order of rinsing, calcination temperature, ml H_2O, drying temperature, and the amount of Al dopant were found to be statistically significant in maximizing the pore volume of DRC samples. The pore volume of DCR samples was affected by order of rinsing, calcination temperature, ml H_2O, H_2O addition speed, calcination ramp rate, and calcination time, as well as several interactions between these factors (Fig. 2). Pore volumes of DRC samples are predicted to be maximized using the maximum ml of H_2O, a high drying temperature, and a low calcination temperature. Pore volumes of DCR samples are predicted to be maximized using the maximum amount of H_2O, a fast H_2O addition speed, a slow ramp rate, a low calcination temperature, and a short calcination time. Prediction Eqs. (5) and (6) can be used to understand factor interactions and determine the pore volume expected under various synthesis conditions.

$$\begin{aligned} DRC\ Pore\ Volume\left(cm^3/g\right) &= 0.28646 \\ &+ 0.001619(ml H_2O) + 0.0006842(dry\ temp) \\ &- 0.000334(calc\ temp) + 0.45857(mol\%Al) \\ R^2 &= 0.865 \quad standard\ deviation = \pm 0.08 \end{aligned} \tag{5}$$

$$\begin{aligned} DCR\ Pore\ Volume\left(cm^3/g\right) &= 0.44548 \\ &+ 0.01862\,(H_2O\ add\ speed) + 0.001532\,(ml H_2O) \\ &- 0.002819\,(calc\ ramp) - 0.00012\,(calc\ temp) \\ &- 0.0011\,(calc\ time) \\ &+ 0.002155\,(H_2O\ add\ speed - 2.0) \\ &\times (ml H_2O - 20) - 0.004226\,(H_2O - 2.0) \\ &\times (calc\ time - 11) + 0.0002402(calc\ ramp - 12) \\ &\times (calc\ time - 11) \\ R^2 &= 0.873 \quad standard\ deviation = \pm 0.10 \end{aligned} \tag{6}$$

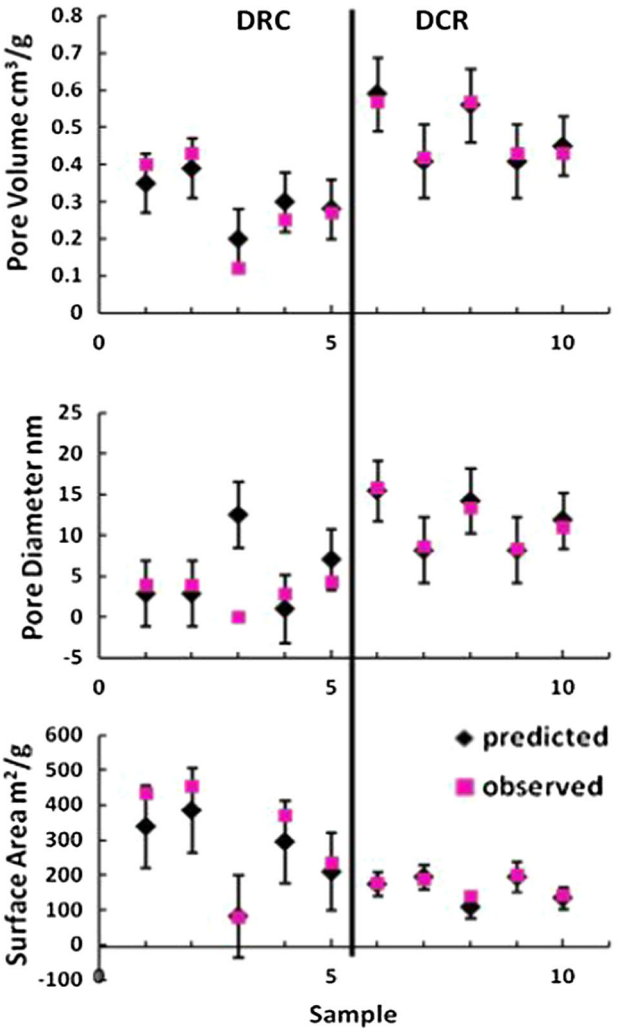

Fig. 3 *Pink squares* correspond to surface areas, pore diameters, and pore volumes observed in confirmation trials and *black diamonds* correspond to predicted values. *Error bars* represent the 95 % confidence intervals on the predictions. Observed values are based on two sample preparations. All values, except pore diameter of Sample 3, were within the 95 % CI of the predictions. Conditions for confirmation trials are listed in Table 5

3.4 Confirmation trials

Confirmation trials were run to verify the accuracy of the prediction equations. The conditions used are listed in Table 5 and the observed and predicted surface areas, pore volumes, and pore diameters (each based on two sample preparations) are shown in Fig. 3. With the exception of the pore diameter of

sample 3, the observed values for all trials were within the 95 % confidence interval of the predicted values. Prediction equations for DCR materials were slightly more accurate and more precise (based on the standard deviations of the experimental errors) than the equations for DRC materials. Smaller pore diameter ranges of 2.93–6.16 nm and larger pore volume ranges of 0.12–0.43 cm^3/g were observed in the DRC confirmatory experiments, compared with the pore diameter ranges of 3.56–14.05 nm and pore volume ranges of 0.13–0.39 cm^3/g observed in DOE 2 (Table 3, used to fit Eqs. (3) and (5)). The different ranges of pore volumes and diameters between DOE 2 trials and the confirmation trials suggest extra variability in the DRC experiments, unaccounted for by the prediction limits of Eqs. (3) and (5), due to unknown changes between DOE 2 trials and confirmatory experiments. Accuracy and precision of the prediction equations could be improved by incorporating additional trials and considering additional synthesis factors.

4 Discussion

The results of this study illustrate the power of using DOEs to (1) optimize the surface area, pore volume, and pore diameter of catalyst supports in a minimum number of experiments and (2) provide a basis for predicting these properties based on experimental conditions. The predictive capability allows for tailoring of the anatase support properties for different applications and an understanding of the range of properties that can be obtained using this synthesis method. The results of this study also provide new insights into the roles of variables in the preparation of aluminum-stabilized anatase.

4.1 The role of preparation variables

The mechanism of the formation of a high surface area material is a complex process involving several steps: nucleation, crystallite growth, polymerization, and agglomeration. In our preparation of anatase, we observed crystallization almost immediately, suggesting that nucleation is a rapid, almost instantaneous process. We observed that much of the crystallization occurs during the short mixing process, but continues to a lesser extent during the drying process. Growth, polymerization, and agglomeration occur throughout the drying and calcination processes. The results of this work provide significant insights into the effects of preparation variables in these important steps in the formation of anatase.

4.1.1 Mixing

The availability of water (Factor B, H_2O addition speed) controls the rates of nucleation and crystallization of anatase. Since water availability affects crystallite formation, H_2O addition speed affected surface area, pore volume, and pore diameter. Slow H_2O addition apparently leads to slower nucleation and controlled growth resulting in small crystallites, small pore diameters, high surface areas, and small pore volumes. Smaller quantities of water (Factor C, ml H_2O) are also associated with low pore volumes. We hypothesize that water adsorbs onto surfaces and stabilizes planes of higher surface energy; however, if less water is available to adsorb onto the surface, high-energy faces are joined in a connected structure to increase stability, resulting in lower pore volumes. In addition, hydrogen bonding is thought to affect self-organization; thus, with less water available and less hydrogen bonding, a more tightly packed and more networked structure with a lower pore volume is formed, while a greater amount of water leads to a more open structure with larger pore volume. The amount of water (Factor C) did not affect the crystallite diameter and consequently did not affect surface area or pore diameter.

4.1.2 Drying

Increasing the drying time (Factor E) leads to larger pores in DCR materials and smaller pores in DRC materials. We hypothesize that gel stiffness and strength increase as drying time increases (due to cross-linking and condensation reactions) and consequently, gels better withstand capillary pressure, which can cause pores to collapse during calcination. Therefore, longer drying times are associated with larger pore diameters, while shorter drying times lead to weaker gels which collapse into smaller pore diameter materials during calcination with no significant change in pore volume. Pore diameters of DRC materials decrease as drying time increases because the large pores formed after long dry times redistribute into smaller, networked pores during rinsing (discussed below). Increasing the drying temperature (Factor F) slightly increases surface area and pore volume of DRC materials. We suspect the amount of dehydration, which occurs during drying and continues during calcination, affects how DRC particles redistribute (discussed below) during the rinsing process. Within the experimental limits tested, the drying temperature had no significant effect on properties of DCR materials (Fig. 2), which were calcined (and further dehydrated) following the drying step.

After drying, crystalline anatase approximately 6–7 nm in diameter is formed. Surface area increases as the amount of Al (Factor J) increases and we therefore hypothesize Al is present as an AlO_x species on the anatase surface. The Al stabilizes anatase by preventing grain growth and rearrangement, thereby delaying the anatase to rutile phase transition.

4.2 DCR

4.2.1 Calcining

Increasing the calcination temperature (Factor H) decreases surface area and pore volume and increases pore diameter because the high calcination temperatures lead to (1) increased crystallinity, densification, grain growth, and agglomeration and (2) loss of surface OH^- species. The effects of calcination temperature on the pore volume and pore diameter were less significant for DCR materials than DRC materials (Fig. 2), indicating that DCR materials are more thermally stable compared with DRC materials. We hypothesize that the larger (6–7 nm) DCR precursors have lower surface energies and therefore sinter less during calcination compared with the smaller (2–3 nm) DRC precursors. Slow calcination ramp rates (Factor G), with slower removal of NH_4Cl and water from the pores (which could act as pillars to support the pore structure at the beginning of the calcination process), resulted in controlled growth and minimally higher surface area and pore volume. Increasing calcination time (Factor I) caused a minimal decrease in pore volume as a result of pores collapsing during prolonged heat treatment.

4.2.2 Rinsing

Rinsing and subsequent drying of calcined anatase materials (DCR materials) does not appear to have any significant effect on the surface area or porosity.

4.3 DRC

4.3.1 Rinsing

Rinsing anatase precursors (DRC route) decreases average crystallite size (from approx 6 to 2 nm). We hypothesize that the smaller crystallites of DRC samples (relative to DCR samples), result from a dissolution and redistribution process during rinsing. Rinsing also affects the location of Al, apparently allowing Al ions to move into empty octahedral sites located in the anatase lattice; this hypothesis is based on observations that increasing Al mol% (Factor J) increases pore volume of DRC materials but does not affect pore volume of DCR materials. Surface Al species and Al^{3+} ions located in octahedral sites apparently stabilize anatase to 400 °C; heat treatment above 400 °C results in grain growth and loss of surface area. XAS studies are needed and presently being pursued to provide information on the mechanism of stabilization in the Al-modified anatase structure.

4.3.2 Calcining

Calcination temperature (Factor H) is the most important factor in the DRC route (Fig. 2). Increasing the calcination temperature results in loss of surface area and pore volume and an increase in pore diameter due to grain growth. Ramp rate and calcination time (Factors G and I) did not significantly impact the properties of DRC materials.

5 Conclusions

We have shown that statistical experimental designs (a) reduce the number of experiments necessary to determine factors and factor interactions that affect surface area, pore volume, and pore diameter, (b) provide a basis for predicting the optimal conditions to obtain the highest surface area and pore volume at the desired pore diameter, and (c) provide inherent statistical measures of confidence in the data obtained.

1. The new DSD used in this study showed correlations among variables and was used to conclusively determine the effects of many different variables while avoiding confounded variables, a drawback of traditional fractional factorial designs.
2. The prediction equations developed in this study match values obtained in confirmatory experiments very well (Fig. 3), providing a high level of predictive capability. Nevertheless, additional experiments could improve the accuracy and precision of the prediction equations. Future studies could include other factors, e.g. analysis of the reaction temperature, reaction pH, aging, rinsing agents, and batch size, as well as extend the limits of the variables examined in this study. We also recognize that a mechanical mixing method would be preferable to the hand grinding method used in this study.
3. Based on the results of this work we can predict and tune the surface area, pore volume, and pore diameter of Al-modified anatase. Both the DRC and DCR routes produce desirable materials with excellent thermal stability. In general, the DRC route produces materials of higher surface area, smaller pore diameter, and smaller pore volume relative to the DCR route, which produces materials of higher pore volume, larger pore diameter, and smaller surface area.

Acknowledgments Funding for this work was provided by the U.S. Department of Energy grant DE-FG02-05ER15666 and the National Science Foundation grant CHE-0959862. We would like to thank Dr Jeff Farrer and the BYU microscopy laboratory for their assistance with TEM imaging.

References

1. M. Haruta, S. Tsubota, T. Kobayashi, H. Kageyama, M.J. Genet, B. Delmon, J. Catal. **144**, 175–192 (1993)
2. H. Imai, M. Date, S. Tsubota, Catal. Lett. **124**, 68–73 (2008)
3. J.K. Edwards, A.F. Carley, A.A. Herzing, C.J. Kiely, G.J. Hutchings, Faraday Discuss. **138**, 225–239 (2008)
4. S.F. Tahir, C.A. Koh, Environ. Sci. Pollut. Res. Int. **3**, 20–23 (1996)
5. J.-J. Shyue, G.M.R. De, J. Am. Chem. Soc. **127**, 12736–12742 (2005)
6. O. Carp, C.L. Huisman, A. Reller, Prog. Solid State Chem. **32**, 33–177 (2004)
7. J. Xu, C.H. Bartholomew, J. Sudweeks, D.L. Eggett, Top. Catal. **26**, 55–71 (2003)
8. M. Nele, A. Vidal, D.L. Bhering, P.J. Carlos, V.M.M. Salim, Appl. Catal. A **178**, 177–189 (1999)
9. Y.-D. Chiang, H.-Y. Lian, S.-Y. Leo, S.-G. Wang, Y. Yamauchi, K.C.W. Wu, J. Phys. Chem. C **115**, 13158–13165 (2011)
10. C.A. McNamara, F. King, M. Bradley, Tetrahedron Lett. **45**, 8239–8243 (2004)
11. M. Naderi, A. Shamirian, M. Edrisi, J. Sol-Gel. Sci. Technol. **58**, 557–563 (2011)
12. V.A. Sakkas, M.A. Islam, C. Stalikas, T.A. Albanis, J. Hazard. Mater. **175**, 33–44 (2010)
13. L. Vanyorek, D. Loche, H. Katona, M.F. Casula, A. Corrias, Z. Konya, A. Kukovecz, I. Kiricsi, J. Phys. Chem. C **115**, 5894–5902 (2011)
14. R.E. Olsen, C.H. Bartholomew, B. Huang, C. Simmons, and B.F. Woodfield, Micropor. Mesopor. Mat. **184**, 7–14 (2013)
15. B. Jones, C.J. Nachtsheim, J. Qual. Technol. **43**, 1–14 (2011)
16. A. Erler, N. Mas, P. Ramsey, G. Henderson, Biotechnol. Lett. **35**, 323–329 (2013)
17. B.F. Woodfield, S. Liu, J. Boerio-Goates, Q. Liu, PCT Int. Appl., WO 2007098111 A2 20070830, 38 pp (2007)
18. C. Wu, M. Hamada, *Experiments: Planning, Analysis, and Parameter Design Optimization* (Wiley, New York, 2000)
19. J. Lawson, *Design and Analysis of Experiments with SAS* (CRC Press, Boca Raton, 2010)
20. J. Lawson, S. Grimshaw, J. Burt, Comput. Stat. Data Anal. **26**, 425–436 (1998)
21. C. Daniel, Technometrics 2 (1960)
22. A.L. Patterson, Phys. Rev. **56**, 978–982 (1939)
23. C. Pierce, J. Phys. Chem. **57**, 149–152 (1953)
24. C. Orr, Jr., J.M. Dallavalle, *Fine Particle Measurement-Size, Surface, and Pore Volume* (Macmillan Co., New York, 1959), p. 353
25. B. Huang, C.H. Bartholomew, B.F. Woodfield, Microporous Mesoporous Mater. **177**, 37–46 (2013)
26. H. Liu, L. Zhang, N.A. Seaton, Langmuir **9**, 2576–2582 (1993)
27. F. Rojas, I. Kornhauser, C. Felipe, J.M. Esparza, S. Cordero, A. Dominguez, J.L. Riccardo, Phys. Chem. Chem. Phys. **4**, 2346–2355 (2002)
28. A.V. Niemark, Stud. Surf. Sci. Catal. **62**, 67–74 (1991)
29. M. Parlar, Y.C. Yortsos, J. Colloid Interface Sci. **124**, 162–176 (1988)
30. P.C. Ball, R. Evans, Langmuir **5**, 714–723 (1989)
31. A.V. Neimark, P.I. Ravikovitch, Microporous Mesoporous Mater. **44–45**, 697–707 (2001)
32. A.V. Neimark, P.I. Ravikovitch, A. Vishnyakov, Phys. Rev. E: Stat. Phys. Plasmas Fluids Relat. Interdiscip. Top. **62**, R1493–R1496 (2000)
33. P.A. Monson, Langmuir **24**, 12295–12302 (2008)
34. H. Chipman, M. Hamada, C.F.J. Wu, Technometrics **39**, 372–381 (1997)
35. P. Woodward, *Bayesian analysis made simple: an excel GUI for WinBUGS* (CRC Press, Boca Raton, 2012)
36. D.J. Spiegelhalter, A. Thomas, N.G. Best, WinBUGS Version 1.2 User Manual, MRC Biostatistics Unit, 1999